ARMA 17-238

Verification of a Calibrated Longwall Model with Field Measurements

Tulu, I.B.[1], Esterhuizen, G.S.[2], Mohamed, K.M.[1] and Klemetti T.M.[2]

[1]Associate Service Fellow, NIOSH Pittsburgh Mining Research Division, Pittsburgh, PA, USA
[2]Principal Research Engineer, NIOSH Pittsburgh Mining Research Division, Pittsburgh, PA, USA

ABSTRACT: A numerical-model-based approach was recently developed by researchers at the National Institute for Occupational Safety and Health (NIOSH) for estimating the changes in both the horizontal and vertical loading conditions induced by an approaching longwall face. In this approach, a systematic procedure is used to estimate the model's inputs. Shearing along the bedding planes is modeled with ubiquitous joint elements and interface elements. Coal is modeled with a newly developed coal mass model at NIOSH's Pittsburgh Mining Research Division (PMRD). The response of the gob is calibrated with back analysis of subsidence data and the results of previously published laboratory tests on rock fragments. The model results were verified with the subsidence and stress data recently collected by PMRD from a longwall mine in the eastern United States, and with published cases studies from both eastern and western U.S. mines.

1. INTRODUCTION

In 2015, there were 40 longwall mines operating in the United States, each producing an average of 4.5 million tons of coal per year. The largest concentrations of longwall faces are found in West Virginia with 13 longwalls, followed by Illinois (7), Pennsylvania (5) and Alabama (5) (Fiskor, 2016).

In 2015, these forty longwall mines supplied 60% of the U.S. underground coal production. This represents a substantial increase from 50% over the previous three years (Sears et al., 2017). During this period, reportable roof fall rates in U.S. longwall mines also increased. Large roof falls that can block the gateroads are not only a ground fall hazard; they disrupt the ventilation system, can block the escapeways, and can increase the potential for elevated methane levels in the gob. To address the recent increase in reportable roof falls, the National Institute for Occupational Safety and Health (NIOSH) Pittsburgh Mining Research Division (PMRD) started a research project to improve ground control in longwall gateroads.

Gateroad layout is primarily determined by the longwall pillar design. Generally, the required dimensions of the pillars around a longwall panel are determined first, which dictates the location of the gateroads relative to the mined panel. The Analysis of Longwall Pillar Stability (ALPS) method is the most accepted design procedure in the United States (Mark, 1992). The ALPS method accounts for local roof geology in the gateroad stability assessment by including the Coal Mine Roof Rating as an input parameter (Mark, 1992). However, ALPS does not address gateroad support design. The key assumption in the ALPS method is that unstable pillars will result in unstable gate entries. However, experience provides many examples of mines where pillar stability and gateroad stability are only loosely correlated (Su et al., 2003).

Gateroad support design is largely empirical, often based on a trial-and-error approach. Gateroad stability and safety can be improved by introducing an engineering-based design approach that specifically considers the rock mass and support response to changes in both the horizontal and vertical loading conditions induced by the approaching longwall face. Such complex stress changes during a longwall retreat can be evaluated with calibrated numerical models, allowing support systems to be designed to accommodate the expected loading conditions.

2. LONGWALL MODEL DEVELOPMENT AND CALIBRATION

Esterhuizen et al. (2010) developed a modeling approach that can be used to provide realistic stress and deformation results along the gateroad chain pillars. In this approach, an "equivalent element" method is used to capture the stress/strain response of the pillars and the immediate roof and floor rocks to model large-scale, three-dimensional retreat mining layouts. One limitation of this approach is that the response of the immediate roof to horizontal stress change during the retreat mining cannot be investigated because only the vertical stress is solved within the equivalent elements. Recently, this approach has been updated for estimating the changes in both the horizontal and vertical loading conditions in the immediate roof of the gateroads. The modified approach uses standard elements to model the pillars, roof, and floor, which provides the full stress tensor, including horizontal stress components in the roof of the coal bed.

2.1. Pillar Strength Modeling

Recently at NIOSH, Mohamed et al. (2015, 2016) developed a coal material model. In this model, the peak strength of the coal is evaluated by the generalized Hoek-Brown failure criterion. The residual stiffness and strength are evaluated by the Fang and Harrison (2002) local degradation model. The dilation of the coal material is defined by the Alejano and Alonso (2005) peak-dilation model.

Mohamed et al. (2016) indicated that the Mohr-Coulomb constitutive model provides a method for describing the dilation behavior of rocks, and it is available in the majority of numerical codes. Therefore, in this model, the equivalent Mohr-Coulomb model parameters derived from the Hoek-Brown criterion are used. This model simulates the peak and post-peak behaviors of the coal material by using a strain-softening, ubiquitous joint model available in the FLAC3D software.

The input parameters used for coal in this paper are summarized in Table 1. In this table "*σci*" is the intact unconfined compressive strength of the coal, and "*m*", "*s*", "*a*" are the peak strength parameters of coal. The parameter "*σc*" represents peak, and "*σcr*" is the residual of the field-scale unconfined compressive strength. "*Nd*" is a coal degradation parameter calculated from tri-axial compression tests of coal samples. This degradation parameter is used to reduce the strength and stiffness of the coal from peak values to residual values in the coal model. "*Ƴpcrit*" is the critical plastic shear strain. The strength of the coal material is reduced until plastic shear strain reaches to this critical value. Coal material fracturing is simulated by adding an implicit cohesion-less ubiquitous joint within the material. Fractures are initiated in those elements which have plastic shear strain equal to or greater than the "fracture plastic shear strain" parameter detailed in Table 1.

Table 1. Input parameters for coal material.

Elastic Properties	*Modulus (GPa)*	3.0
	Poisson's Ratio	0.25
Strength Parameters	*σci (MPa)*	20
	m	1.52
	s	0.013
	a	0.5
	σcr (MPa)	0.30
	σc (MPa)	2.28
Degradation Parameters	*Nd*	0.503
	Ƴpcrit	0.26
Ubiquitous Joint Friction Angle		25
Fracture Plastic Shear Strain		0.0275

The coal model was originally developed to simulate the stress/strain behavior of coal pillar ribs. This model also simulates the stress/strain behavior of full coal pillars satisfactorily, as demonstrated below.

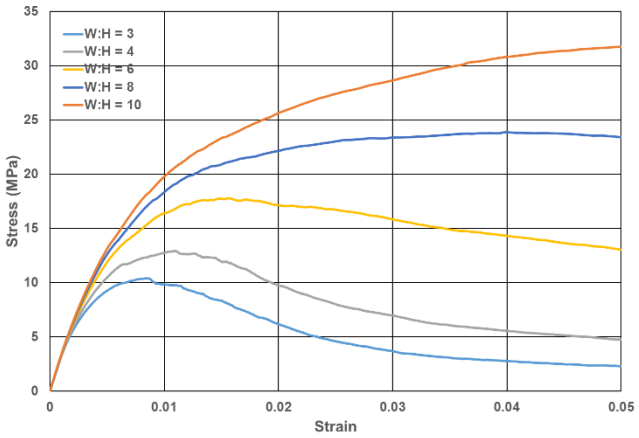

Fig 1. Stress-strain curves obtained from a calibrated coal model.

To compare the stress-strain behavior of the pillars generated with the coal model of Mohamed et al. (2016) to results obtained by Esterhuizen et al. (2010), numerical models were created in which portions of the roof strata, the coal pillar, and the floor strata were simulated. The same boundary conditions and model geometries used by Esterhuizen et al. (2010) were modeled. Figure 1 shows the resulting stress-strain curves obtained from the coal models with different pillar width-to-height ratios. The stress-strain behavior presented in Figure 1 is similar to the results published by Esterhuizen et al. (2010). Post-peak stress/strain behavior was slightly different. For the width-to-height ratios below 8, the pillars exhibit a strain-softening behavior. For the width-to-height ratios above 8, the pillars exhibit a strain-hardening behavior.

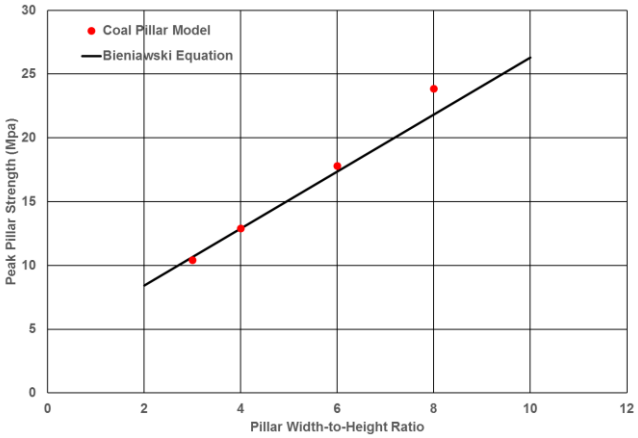

Fig 2. Pillar strength results obtained by numerical models after calibrating the models to the empirical pillar strength equation.

The peak pillar strengths simulated by the numerical models are compared with the empirical Bieniawski pillar strength equation in Figure 2. The results show good agreement between the model calculations and the empirical equation.

2.2. Gob Response Modeling

It is important to simulate the gob response accurate to simulate the load distribution along the gateroad entries. Esterhuizen et al. (2010) indicated that gob modeling can follow two approaches: 1) explicitly model the gob formation process so that variations in geology and loading conditions can be studied, 2) implicitly model the gob compaction and load distribution to accurately model load redistribution to gateroad pillars and surrounding rock. As in Esterhuizen et al. (2010), the second approach is used in this paper to simulate the behavior of the gob.

As indicated by Pappas and Mark (1993) laboratory tests on shale and sandstone fragments showed that the stress-strain response of caved material should follow a strain-hardening curve. Pappas and Mark (1993) used the hyperbolic function derived by Salamon (1990) to fit test results, and they found that this function sufficiently simulates the strain-hardening gob response.

$$\sigma = \frac{a \times \varepsilon}{b - \varepsilon} \qquad (1)$$

where:

σ = vertical gob stress (MPa).
ε = vertical gob strain.
b = maximum strain parameter related to void ratio.
a = gob stress where ε = b/2 (MPa).

Esterhuizen et al. (2010) calibrated the hyperbolic equation (Eq. 1) by matching the model results with subsidence profiles that were calculated from the Surface Deformation Prediction Software (SDPS) (Newman et al., 2001). To assist selecting appropriate gob parameters, they followed the same approach used by SDPS, in which the gob is characterized by the ratio of the thicknesses of "strong" and "weak" rocks in the overburden. They classified weak rocks as shales and clay stones that have a field scale Uniaxial Confining Strength (UCS) of less than 40 MPa, while limestone, sandstone, and siltstone have a field scale UCS above 40 MPa and would be classified as strong rocks. Esterhuizen et al. (2010) found that 44% represents the maximum vertical strain parameter "*b*," which provides the initial bulking factor of 1.79. They also found four different "*a*" parameters for four gob types that were classified with a ratio of strong to weak rocks in the overburden: 1) weak (25%), 2) moderate (35%), 3) strong (50%), and 4) very strong (65%). The strong and moderate gob curves derived by Esterhuizen et al. (2010) are almost identical to laboratory best-fit curves for sandstone and shale materials that were published by Pappas and Mark (1993).

Su (1991) simulated the behavior of the gob which is assumed to be formed under an initial bulking factor of 1.5, representing a maximum strain of 33% and a caving height equal to three times the mining height. Su (2016) used this approach very successfully for many years for estimating surface subsidence and pillar stresses for a number of longwall mines. In addition, it was found that the gob parameters used by Su (1991) give close stress-strain values to the weak/moderate overburden gob response curves published by Esterhuizen et al. (2010), up to a gob compaction of 28%.

Maximum vertical strain is related to initial bulking factor (or initial void ratio). The average initial bulking factor of the test samples used by Pappas and Mark (1993) are: 1) 1.80 for shale, 2) 1.74 for sandstone, and 3) 1.87 for strong sandstone. Pappas and Mark used photographs from several gob sites from the headgate entries to estimate the distribution of size of the rock in the gob. These size distributions were scaled down to laboratory scale sample size. These values of the bulking factor represent fully rotated and dislocated blocks, which represents the maximum bulking potential of the broken rock. In a mine gob, the void ratio will decrease with distance above the floor (Esterhuizen and Karacan, 2007). A value of 1.5 appears to be good representation of average bulking factor.

In this paper the gob represents only the caved material and excludes fractured rock above the caved zone. Based on the above discussions and the calibration of the gob response curve with subsidence data, the gob parameters proposed by Esterhuizen et al. (2010) were modified by assuming the gob was formed under an initial bulking factor of 1.5, which represents a maximum strain of 33% and a caving height equal to three times the mining height measured from the floor. This approach also provides reasonable estimates of the subsidence. Two types of gob parameters are suggested for strong overburden and weak overburden. Figure 3 shows the stress-strain behavior of these two gob types and a comparison to the tests results

of Pappas and Mark (1993). Table 2 shows the gob parameters for these two curves.

In the model, strain-hardening gob behavior is simulated by updating the elastic modulus of each zone with the expected tangent modulus. The expected tangent modulus can be calculated by taking the derivative of Eq. 1 with respect to vertical strain (Eq. 2). This task is performed by using the FISH option of the FLAC3D software.

$$\frac{d\sigma}{d\varepsilon} = E(\varepsilon) = \frac{a \times b}{(b-\varepsilon)^2} \quad (2)$$

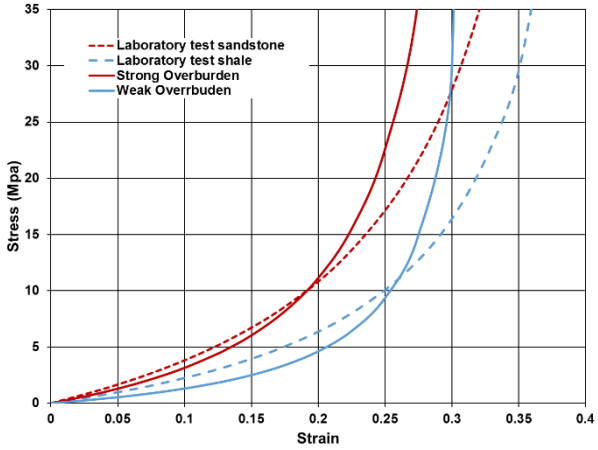

Fig 3. The stress/strain curve for gob materials used in the FLAC3D model and results of laboratory tests on gob materials, after Pappas and Mark (1993).

Table 2. Parameters for modeling various gob types.

Overburden Type	***a* (MPa)**	**b**
Weak	3	0.33
Strong	7.24	0.33

2.3. Overburden Properties

Esterhuizen et al. (2010) published the suggested rock elastic, intact strength, and bedding strength properties for modeling large-scale coal measure rock in the United States. Some modifications and corrections were made to the data published by Esterhuizen et al. Updated properties are presented in Table 3 and Table 4.

UCS values in Table 3 are laboratory scale values. The field value of the *UCS* is estimated by multiplying the laboratory value with 0.58 (Esterhuizen et al., 2010; Hoek and Brown, 1980). Poisson's ratio was set to 0.25. For sandstone and shale, the elastic modulus (E) is estimated from Eq. 3, and for limestone, the elastic modulus is estimated from Eq. 4. These equations were driven from the regression analysis of a large number of UCS tests. In Eq. 3 and Eq. 4, the *UCS* is the laboratory scale value in MPa and the resultant elastic modulus is in GPa.

$$E = 0.143 \times UCS + 6.16 \quad (3)$$

$$E = 0.1162 \times UCS + 15.24 \quad (4)$$

The friction angles are determined from the database of tri-axial tests (Esterhuizen et al., 2010). The friction values are also assumed to be the same in the laboratory and field scales. The cohesion values listed in Table 3 are field scale values and calculated by using Eq. 5.

$$C = \frac{UCS_{field} \times (1 - \mathrm{Sin}(\varphi))}{2 \times Cos(\varphi)} \quad (5)$$

where;

C = field scale cohesion.
φ = friction angle.
$UCS_{field} = UCS_{lab} \times 0.58$

Tensile strengths (σ_t) are calculated by using Eq. 6.

$$\sigma_t = 0.1 \times UCS_{field} \quad (6)$$

Table 3. Suggested intact rock properties.

Type	*UCS (MPa)*	*E (GPa)*	*Friction Angle (deg.)*	*Cohesion (MPa)*	*Tensile Strength (MPa)*
Limestone	140	31.51	42	18.08	8.12
	100	26.86	42	12.91	5.80
	80	24.54	40	10.82	4.64
Sandstone	120	23.32	42	15.49	6.96
	100	20.46	40	13.52	5.80
	80	17.60	37	11.57	4.64
	60	14.74	35	9.06	3.48
	40	11.88	30	6.70	2.32
Shale	80	17.60	32	12.86	4.64
	60	14.74	30	10.05	3.48
	40	11.88	25	7.39	2.32
	30	10.45	20	6.09	1.74
	20	9.02	20	4.06	1.16
	10	7.59	20	2.03	0.58
	5	6.88	20	1.02	0.29

Bedding strength parameters summarized in Table 4 were derived by Esterhuizen et al. (2010). Bedding tensile strength was set to 10% of the field-scale UCS. Esterhuizen et al. (2010) indicated that bedding friction angles may seem to be small compared to small-scale laboratory strength tests, but the presence of weak clay materials, especially in the shale beds, can have a significant impact on the overall shear resistance of a bedding plane.

The matrix cohesion and tensile strength decreased from their peak values given in Table 3 to a residual value of 10% of peak over 5 millistrains of plastic strain (Zipf, 2007). The matrix friction angle remains constant at the values shown in Table 3. The stress-strain behavior of the bedding planes assumed to be elastic perfectly plastic.

Table 4. Suggested bedding strength properties.

Type	*Cohesion (Mpa)*	*Friction (deg.)*	*Tension (Mpa)*
Limestone	9.47	32	0.81
	7.55	30	0.58
	6.70	28	0.46
Sandstone	8.11	30	0.70
	6.76	30	0.58
	6.04	27	0.46
	4.53	25	0.35
	3.35	20	0.23
Shale	2.96	10	0.46
	2.44	7	0.35
	1.78	7	0.23
	0.50	7	0.17
	0.30	5	0.12
	0.20	5	0.06
	0.10	5	0.03

Interfaces between the geological layers in the overburden were modeled with the interface elements. This is the major difference from Esterhuizen et al. (2010). Coulomb's criterion was used to define the limiting shear strength of the interfaces. As described by Su (1991, 2016) the coefficient of friction of interfaces was set to 0.25. Joint shear stiffness was set to 0.5 GPa/m and normal stiffness was set to 10 times the shear stiffness.

3. VERIFICATION OF UPDATED MODEL WITH PUBLISHED CASE HISTORIES

Case histories used by Esterhuizen et al. (2010) were again used to verify the updated modeling methodology and input parameters. In addition, subsidence and stress data recently collected by the Pittsburgh Mining Research Division (PMRD) from a longwall mine in West Virginia were used to verify the model results.

3.1. Supercritical Longwall Panel from the Pittsburgh Coal Seam.

The first case study is from the Pittsburgh coal seam where detailed subsidence measurements have been made (Zimmerman and Fritschen, 2007; Esterhuizen et al., 2010). The depth of cover is 200 m, and the panel width is 350 m. The gateroad system is a three-entry with 24-m-wide chain pillars. The mining height is 1.7 m.

The behavior of the gob, which is assumed to be formed under an initial bulking factor of 1.5, was simulated with the weak overburden strain-hardening gob parameters detailed in Table 2. The coal material was simulated with the material properties detailed in Table 1. The overburden in this area consists of alternating layers of shale, siltstone, sandstone, and limestone. Fifty-two different layers with thicknesses ranging from 2.5 m to 15 m were used to simulate the overburden. The strongest rock layer was limestone with a laboratory-scale UCS of 100 MPa, and the weakest rock was shale with a 30 MPa (Table 3 and Table 4). Thickness weighted average of the laboratory-scale UCS of the overburden was 52 MPa.

Figure 4 shows the comparison of the subsidence results calculated by the model and published by Esterhuizen et al. (2010). The model simulates the maximum subsidence very close to the field measurements. The accuracy of the subsidence curve is also satisfactory. The model-calculated subsidence results confirm that the model simulates the gob compaction satisfactorily for this case study.

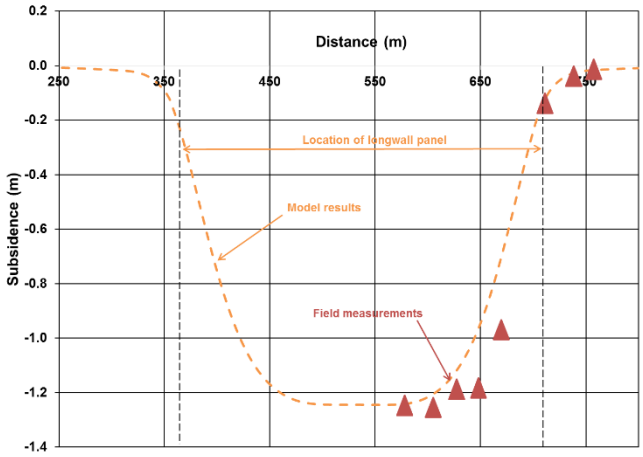

Fig 4. Comparison of model-calculated subsidence results with field measurements.

The average stress on the chain pillars calculated by the model and by the ALPS empirical equations (Mark, 1992) are summarized in Table 5. The model-calculated average stress on the abutment pillars is slightly higher than calculated by ALPS. The abutment angle calculated from the model results is 27.8°, which is higher than the abutment angle of 21° that is assumed by ALPS. The 6.8° difference in abutment angle increased the average stress on the pillar-1 by 3 MPa and less than 0.28 MPA on the pillar-2. This difference will reduce the stability factor of the pillar-1 by only 8.5%, which is insignificant.

Table 5. Average stress on the chain pillars and abutment angles.

	Average Vertical Stress (MPa)	
	Pillar-1	*Pillar-2*
ALPS	12.29	7.85
Model	15.24	8.13

3.2. Subcritical Longwall Panel in Utah.

The second case study is from a longwall mine in Utah where the U.S. Bureau of Mines (Allgaier, 1988)

measured the subsidence profiles. The subsidence was measured for five years during the mining of four panels. The average depth of cover was about 450 m, and the average mining height was 3 m. The subsidence over the first two panels is simulated with the model, and results are compared with the field data.

The first panel was 146-m wide and the second panel was 164-m wide. Panels were separated with a three-entry gateroad system. Pillars had the width-to-height ratio of 3.2 and were yielding pillars. The overburden in this area consisted of alternating layers of interbeds of sandstone/shale, massive Castlegate sandstone, siltstone, and mudstone. Forty-eight different layers with thicknesses ranging from 3 to 45 m were used to simulate the overburden. The thickness weighted average of the laboratory-scale UCS of the overburden is 90 MPa.

The behavior of the gob, which is assumed to be formed under an initial bulking factor of 1.5, was simulated with the strong overburden strain-hardening gob parameters detailed in Table 2. Coal material was simulated with the material properties detailed in Table 1.

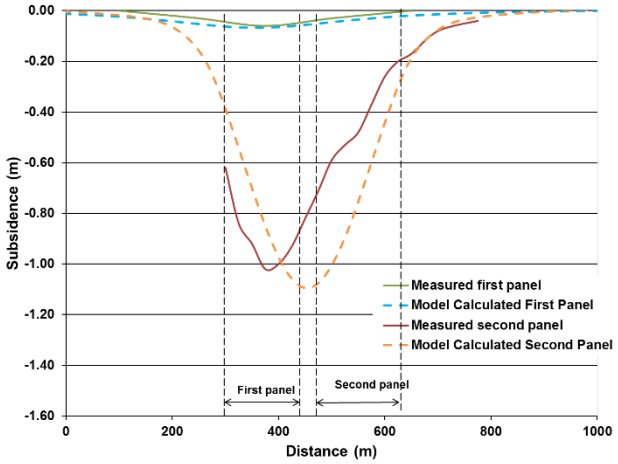

Fig 5. Comparison of model-calculated subsidence results with field measurements.

Figure 5 shows the comparison of the subsidence results calculated by the model and published by Allgaier (1988). The model simulates the maximum subsidence very close to the measurements after first-panel mining and slightly higher after second-panel mining. Although there are some differences between field data and model calculations, accuracy of the subsidence curve is satisfactory, particularly the ability to predict the large difference between first- and second-panel mining.

3.3. Longwall Mine in West Virginia.

The third and the last case study is from a mine in West Virginia. Stress data recently collected by PMRD and the mine provided the subsidence data. Depth of cover varies from 100 m to 230 m along the longwall panels. Typical depth is in the 180-m range. Mining height is 2 m.

The overburden in this area consists of alternating layers of shale, sandstone, and limestone. Sixty-one different layers with thicknesses ranging from 1 m to 10 m were used to simulate the overburden. The thickness weighted average of the laboratory-scale UCS of the overburden is 54 MPa. The behavior of the gob, which is assumed to be formed under an initial bulking factor of 1.5, was simulated with the weak overburden strain-hardening gob parameters detailed in Table 2. The coal material is simulated with the material properties detailed in Table 1.

Figure 6 shows the comparison of the subsidence results calculated by the model and the field data. The model simulates the maximum subsidence very close to the field measurements. The shape of the subsidence curve is also satisfactory. The model-calculated subsidence results confirm that the model simulates the gob compaction satisfactorily for this case study.

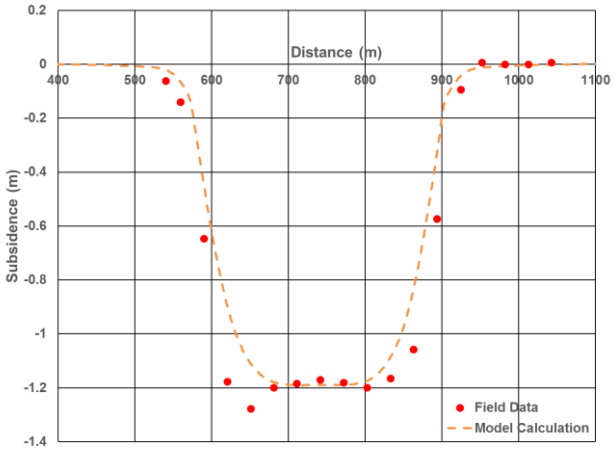

Fig 6. Comparison of the subsidence measurements with model results.

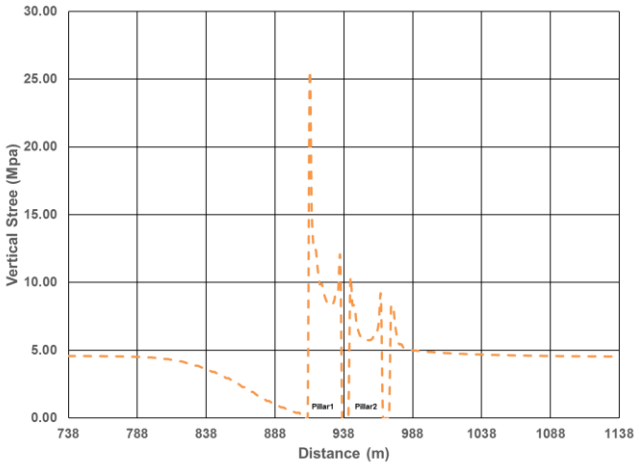

Fig 7. Model-calculated vertical stress distribution.

Figure 7 shows the stress distribution along the gob and gateroad pillars after the first panel is mined. PMRD installed six CSIRO Hollow Inclusion cells into the roof rock along the pillar-2 and the solid coal during the development stage. Also, in-situ stresses were measured with overcoring of two cells. Therefore, both in-situ

stresses before the mining of the panel and the stress change during the mining were monitored.

Figure 8 shows the model-predicted and measured stress profile adjacent to the center entry between the two chain pillars. Red dots show the measured total vertical stress after first-panel mining. The dotted orange lines show the total vertical stress calculated by the model after first-panel mining. Figure 8 shows that the model predicts total vertical stress that is close to the field measurements.

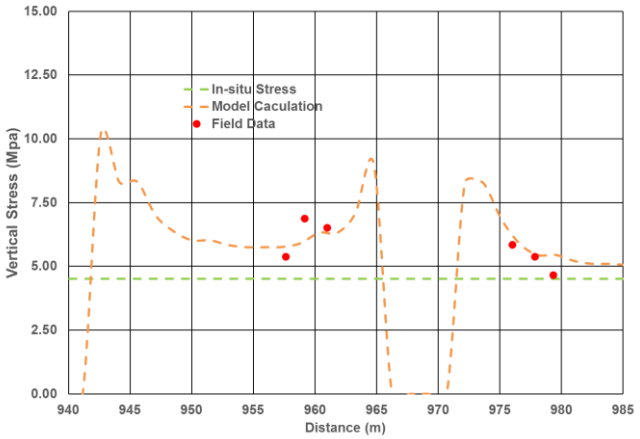

Fig 8. Comparison of field-measured and model-calculated vertical stress.

4. CONCLUSION

This paper summarizes and verifies an updated approach to Esterhuizen et al., (2010) with published case studies and subsidence/stress data recently collected by the Pittsburgh Mining Research Division (PMRD) from a longwall mine in the eastern United States. The model results show that the response of coal measure rocks due to longwall mining can be simulated satisfactorily with this updated approach. The paper also provides a basic set of input data and a modeling approach for overburden rocks, coal material, and gob material.

Numerical models can be a useful tool for longwall gateroad design only if they approximate the response of the overburden strata, gob, and chain pillars within a certain accuracy. The accuracy of the model results can only be quantified by the available field measurements. In the future, more case studies will be used to verify the modeling approach used in this paper.

DISCLAIMER

The findings and conclusions in this paper are those of the authors and don not necessarily represent the views of the National Institute for Occupational Safety and Health (NIOSH). Mentioning and company name, product or software does not constitute endorsement by NIOSH.

REFERENCES

1. Alejano, L.R., and E. Alonso. 2005. Considerations of the dilatancy angle in rocks and rock masses. *Int. J. Rock Mech. Min. Sci.* 42(4):481–507.
2. Allgaier, F.K. 1988. *Surface Subsidence Over Longwall Panels in the Western United States – Final Results at the Deer Creek Mine, Utah*. U.S. Bureau of Mines IC 9194.
3. Esterhuizen, G.S., C. Mark, and M.M. Murphy. 2010. Numerical model calibration for simulating coal pillars, gob and overburden response. In *Proceedings of the 29th International Conference on Ground Control in Mining, Morgantown, 25–27 July 2010*, pp. 1 - 12.
4. Esterhuizen, G.S., and C.O. Karacan. 2007. A methodology for determining gob permeability distributions and its application to reservoir modeling of coal mine longwalls. In *Proceedings of the Society for, Mining, Metallurgy and Exploration, Inc. Annual Conference*, Denver, Colorado, 2007.
5. Fang, Z. and Harrison J.P. 2002. Development of a local degradation approach to the modeling of brittle fracture of heterogeneous rocks. *Int. J. Rock Mech. Min. Sci.* 39: 443–457.
6. Fiskor S. 2016. U.S. Longwall Census, Coal Age, February, 2016. pp 26-32.
7. Hoek, E. and E.T. Brown. 1980. Underground Excavations in Rock. Inst. Min. Metallurgy, London, 527 p.
8. Mark, C. 1992. Analysis of longwall pillar stability (ALPS): an update. *In Proceedings of the Workshop on Coal Pillar Mechanics and Design. Bureau of Mines IC 9315, pp. 238–249.*
9. Mohamed, K.M., I.B. Tulu, and T. Klemetti. 2015. Numerical simulation of deformation and failure process of coal-mass. In *49th US Rock Mechanics/Geomechanics Symposium*, American Rock Mechanics Association.
10. Mohamed, K.M., I.B. Tulu, and M.M. Murphy. 2016. Numerical model calibration for simulating coal ribs. *Proceedings of the Society for, Mining, Metallurgy and Exploration, Inc. Annual Conference, Phoenix, Arizona, 2016.*
11. Newman, D.A., Z. Agioutantis and M. Karmis. 2001. SDPS for windows: an integrated approach to ground deformation prediction. In *Proceedings of the 20th International Conference on Ground Control in Mining, Morgantown, 25 -27 July 2001*, pp. 157 -162.
12. Pappas, D.M. and C. Mark. 1993. *Behavior of Simulated Gob Material.* U.S. Bureau of Mines RI 9458.
13. Salamon M.D.G. 1990. Mechanism of caving in longwall coal mining. *In Proceedings of the 21th U.S. Rock Mechanics Symposium, Denver CO, A.A. Balkema, pp. 161-168.*
14. Sears, M.M., I.B. Tulu, and G.S. Esterhuizen 2017. Overview of Current Longwall gateroad support

practices. In *Proceedings of the Society for, Mining, Metallurgy and Exploration, Inc. Annual Conference, Denver, Colorado, 2017.*

15. Su, D.W.H. 1991. Finite Element Modeling of Subsidence induced by underground coal mining: the influence of material nonlinearity and shearing along existing planes of weakness. In *Proceedings of the 10th International Conference on Ground Control in Mining, Morgantown, 25 -27 July 1991*, pp. 287 -300.

16. Su, D.W.H., D.J. Draskovich, and E.P. Thomas. 2003. Pillar design and roof support for controlling longwall headgate subject to high horizontal stresses. In *Proceedings of the 22nd International Conference on Ground Control in Mining, Morgantown, 25 -27 July 2003*, pp. 1–10.

17. Su, D.W.H. 2016. Personal communications.

18. Zimmerman, K. and R. Fritschen. 2007. Study about the dynamic influence of longwall mining in the U.S. on surface structures. In *Proceedings of the 26th International Conference on Ground Control in Mining, Morgantown, 25–27 July 2007*, pp. 79–84.

19. Zipf R. K. 2007. Numerical modeling procedures for practical coal mine design. *In Proceedings of the International Workshop on Rock Mass Classification in Underground Mine Design*, NIOSH IC 9498, pp. 153-162.